S-scheme *α*-Fe_2O_3/Cu_2O photocatalyst for enhanced primary amine oxidative coupling reaction under visible light

Zhen Li[a,b,1], Shan Ye[a,1], Ping Qiu[a], Xiaoyuan Liao[a], Yue Yao[a], Jingzhao Zhang[c], Yan Jiang[a] and Shuxiang Lu[a,b,*]

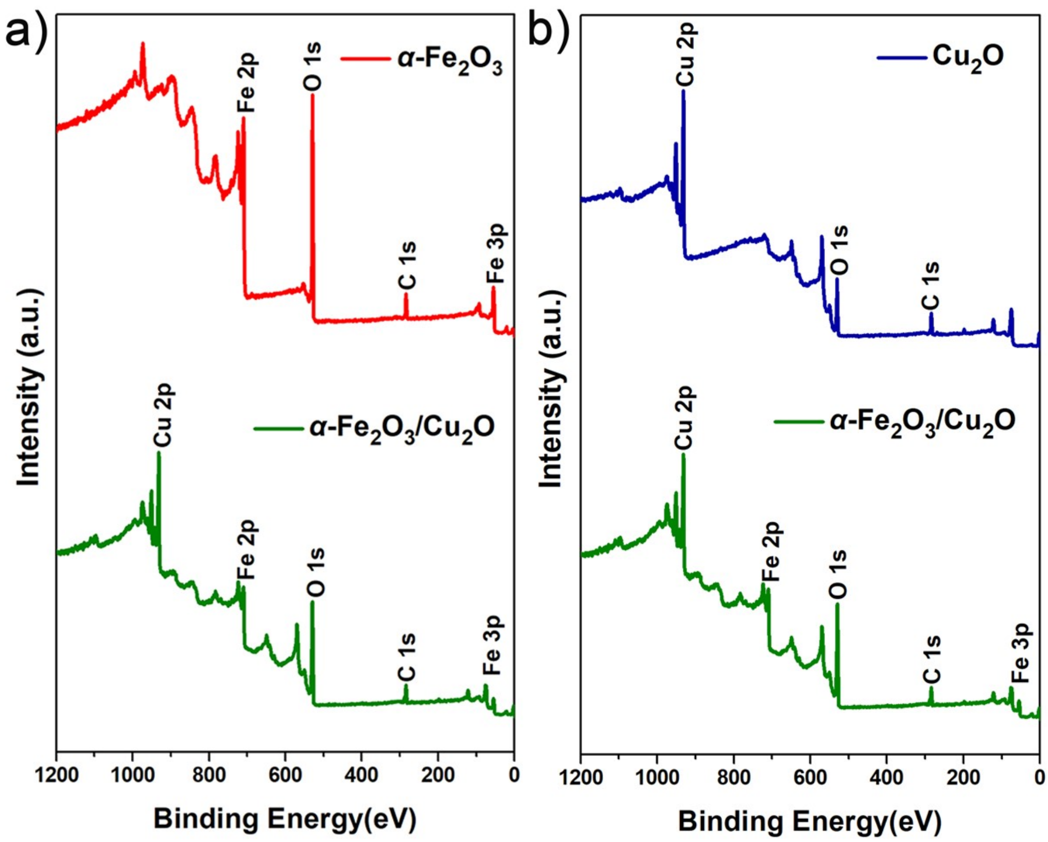

Fig. S1 Survey of XPS.

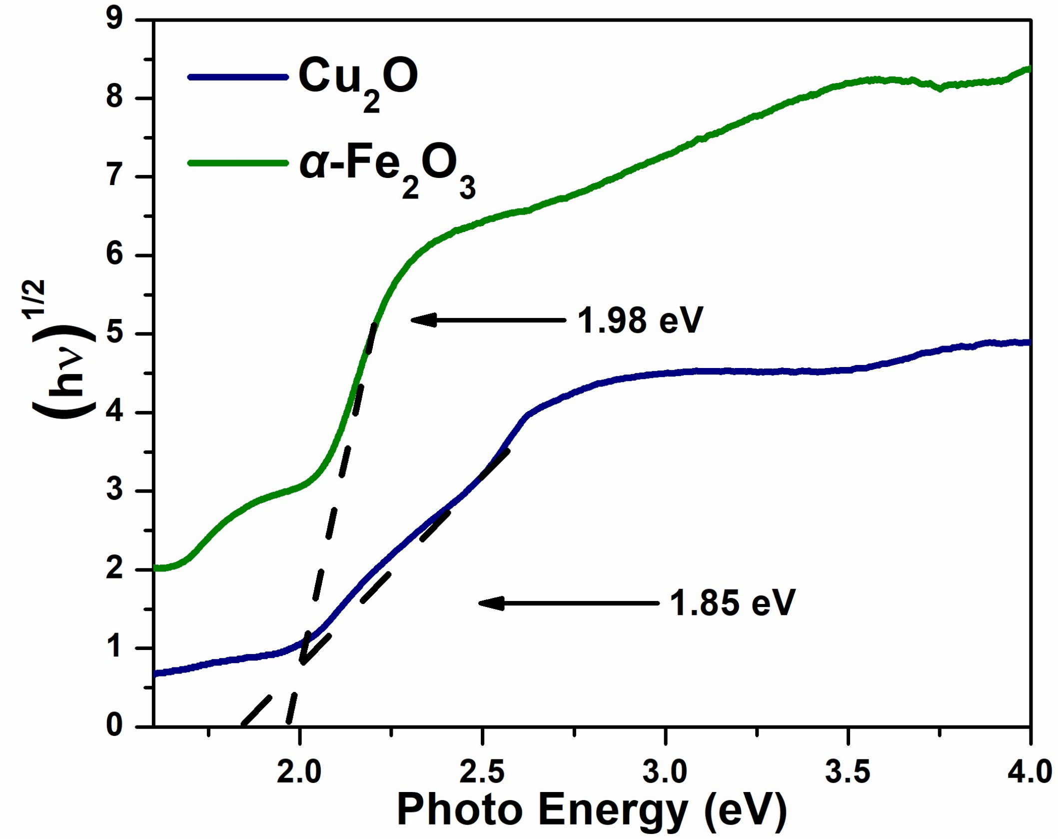

Fig. S2 Estimated band gaps of pure Cu_2O and α-Fe_2O_3.

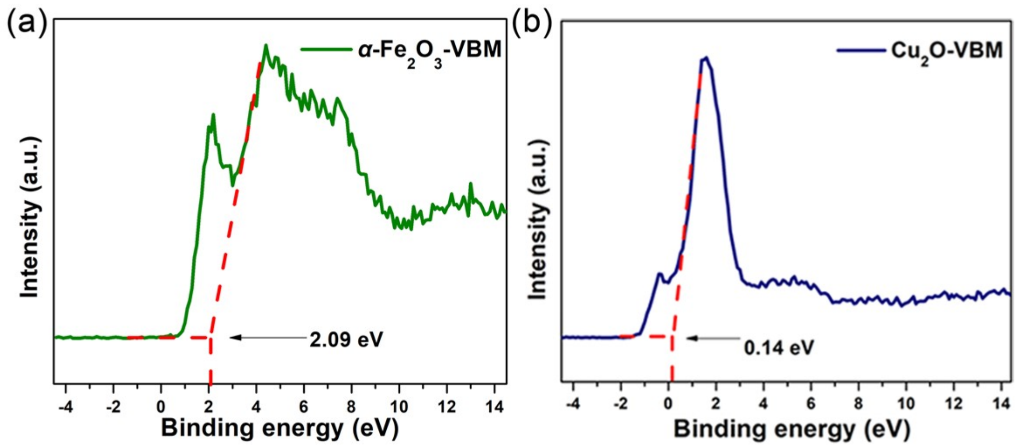

Fig. S3. Valence-band XPS spectra of pure α-Fe_2O_3 (a) and Cu_2O (b).

The transfer process of electron-hole pairs is further determined by analyzing the band positions of α-Fe_2O_3 and Cu_2O semiconductors. Fig. S2 is the K-M function calculation of the UV-Vis diffuse reflectance spectra of pure α-Fe_2O_3 and Cu_2O. In the figure, the intercept between the tangent line and the abscissa is the semiconductor band gap (Eg). The band gaps of α-Fe_2O_3 and Cu_2O are 1.98 eV and 1.85 eV, respectively.

From Fig. S3a and S3b, the valence band potential can be estimated to be 2.09 and 0.14 eV [1,2], and combined with the band gap results, the conduction band potential can be obtained to be 0.11 and −1.71 eV, respectively, using the band gap formula ($E_g = E_{VB} - E_{CB}$). It can be clearly seen that the energy of α-Fe_2O_3 and Cu_2O overlap, so they can form an effective Z-scheme structure.

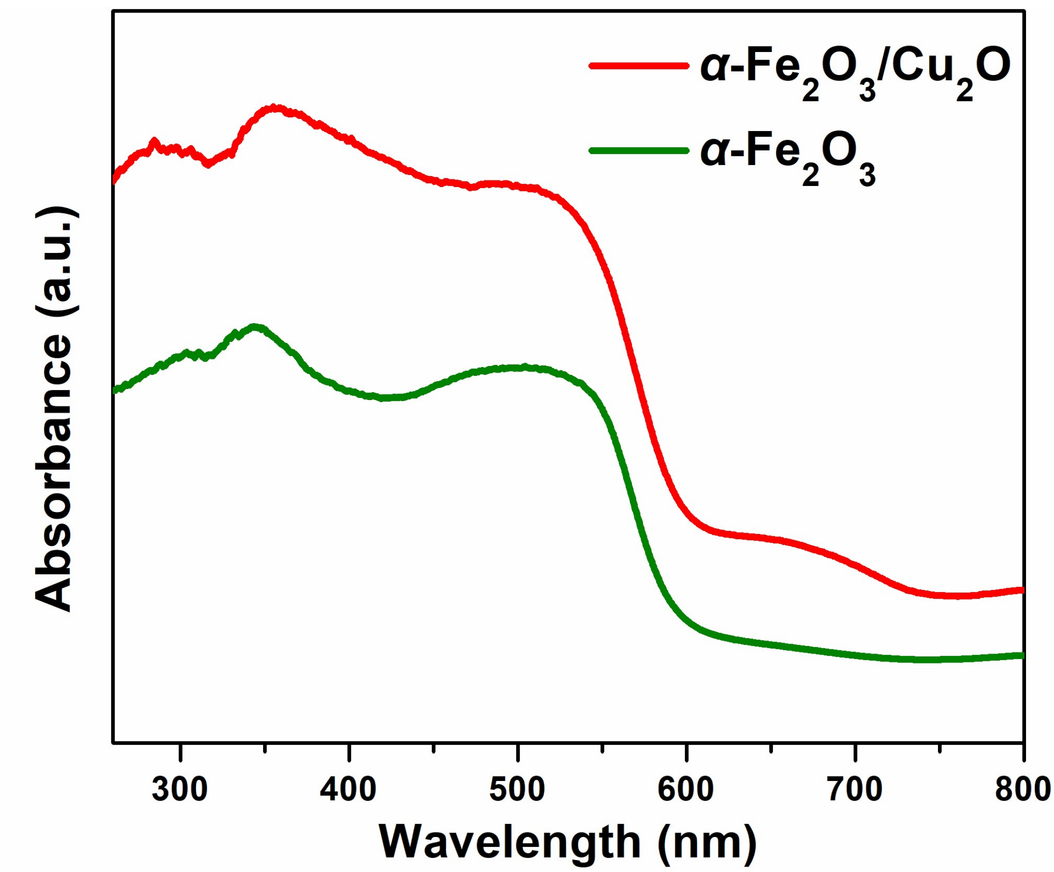

Fig. S4 UV-vis diffuse reflectance spectra of α-Fe_2O_3 and α-Fe_2O_3/Cu_2O composite.

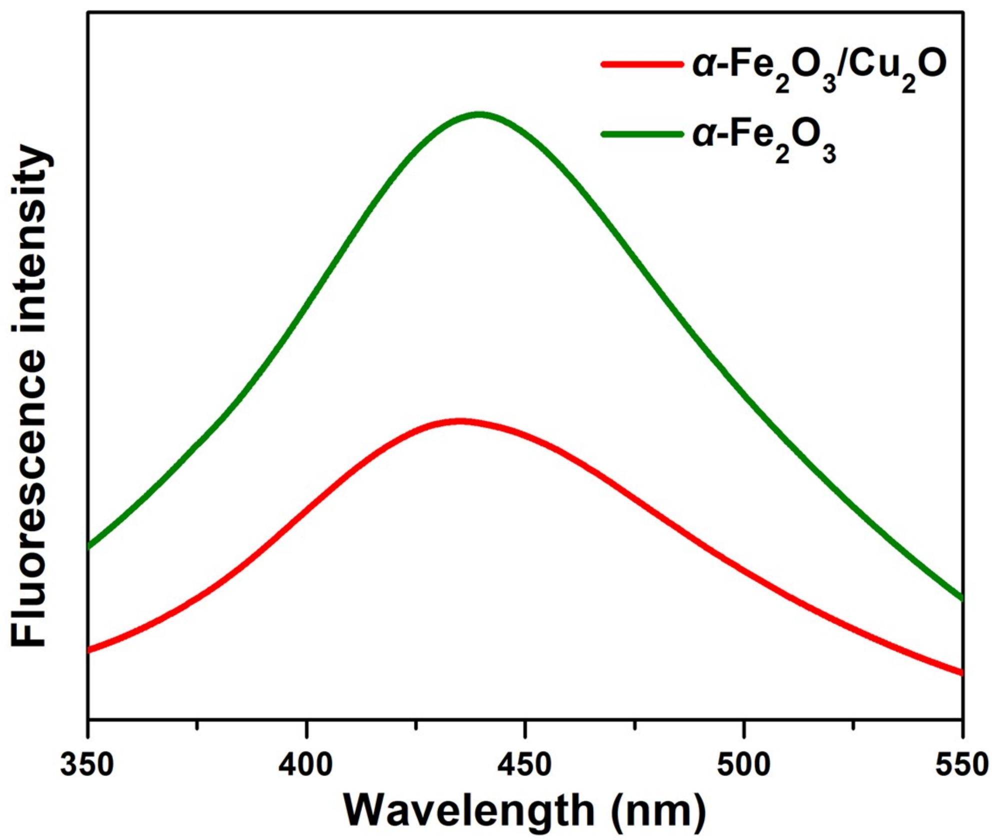

Fig. S5 PL spectra of α-Fe_2O_3 and α-Fe_2O_3/Cu_2O composite.

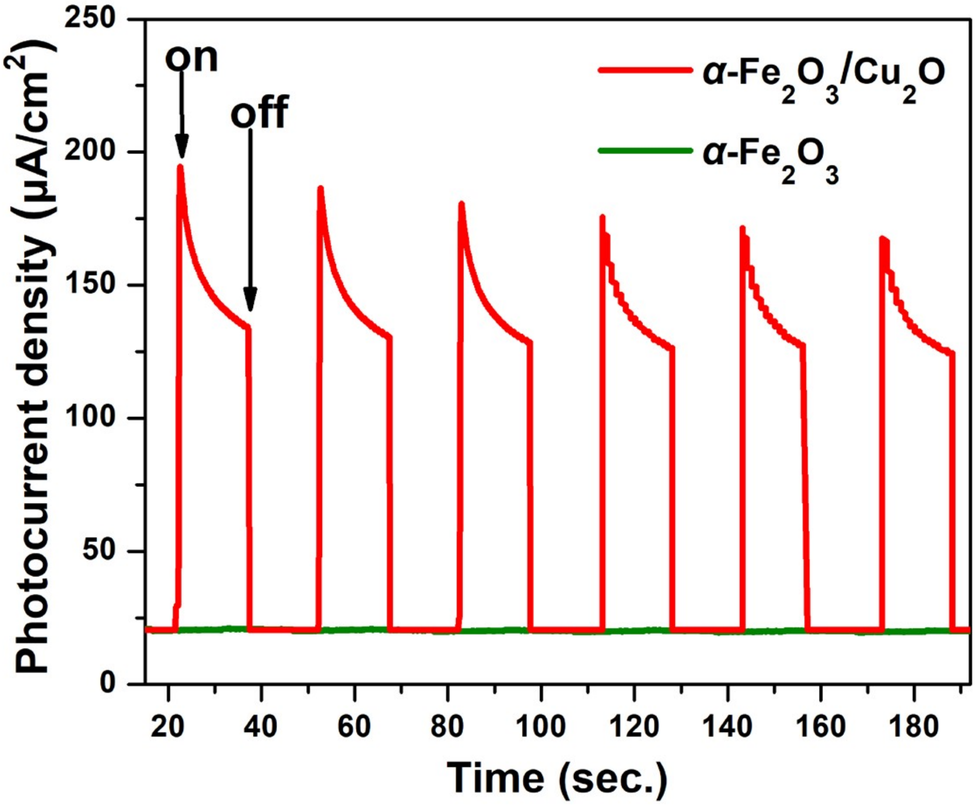

Fig. S6 Transient photocurrent density of α-Fe_2O_3 and α-Fe_2O_3/Cu_2O composite.

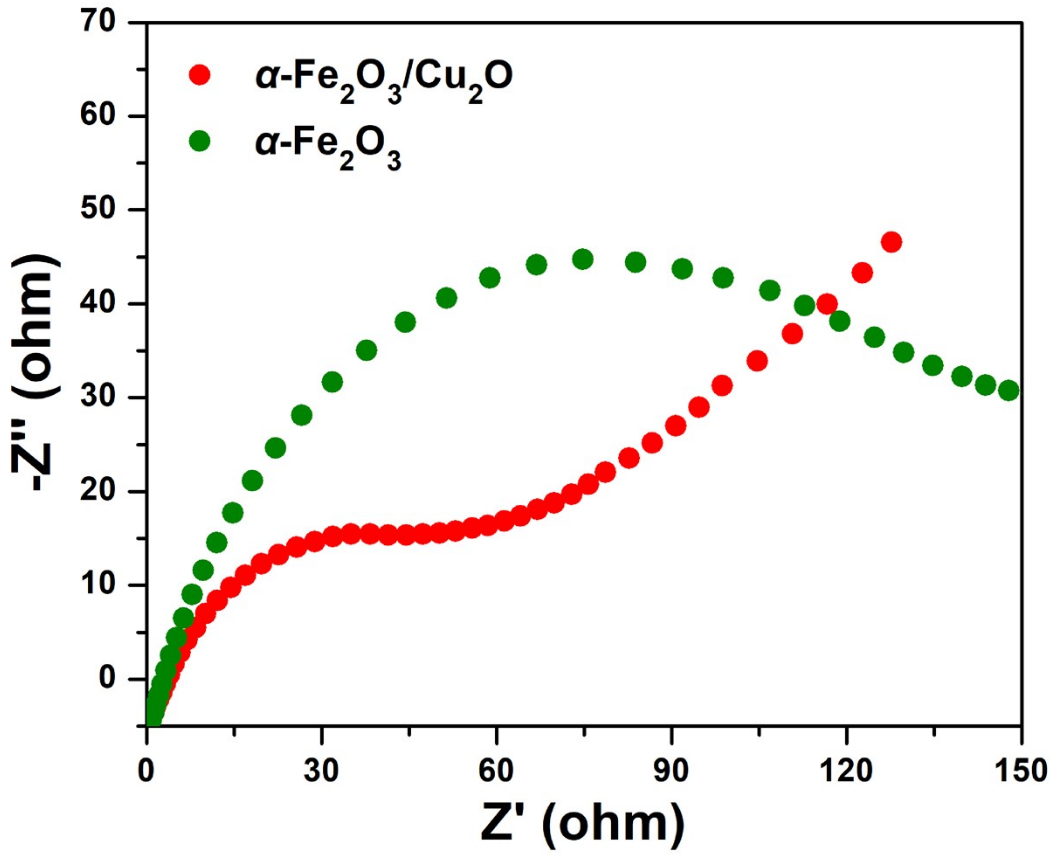

Fig. S7 EIS Nyquist plots of α-Fe_2O_3 and α-Fe_2O_3/Cu_2O composite.

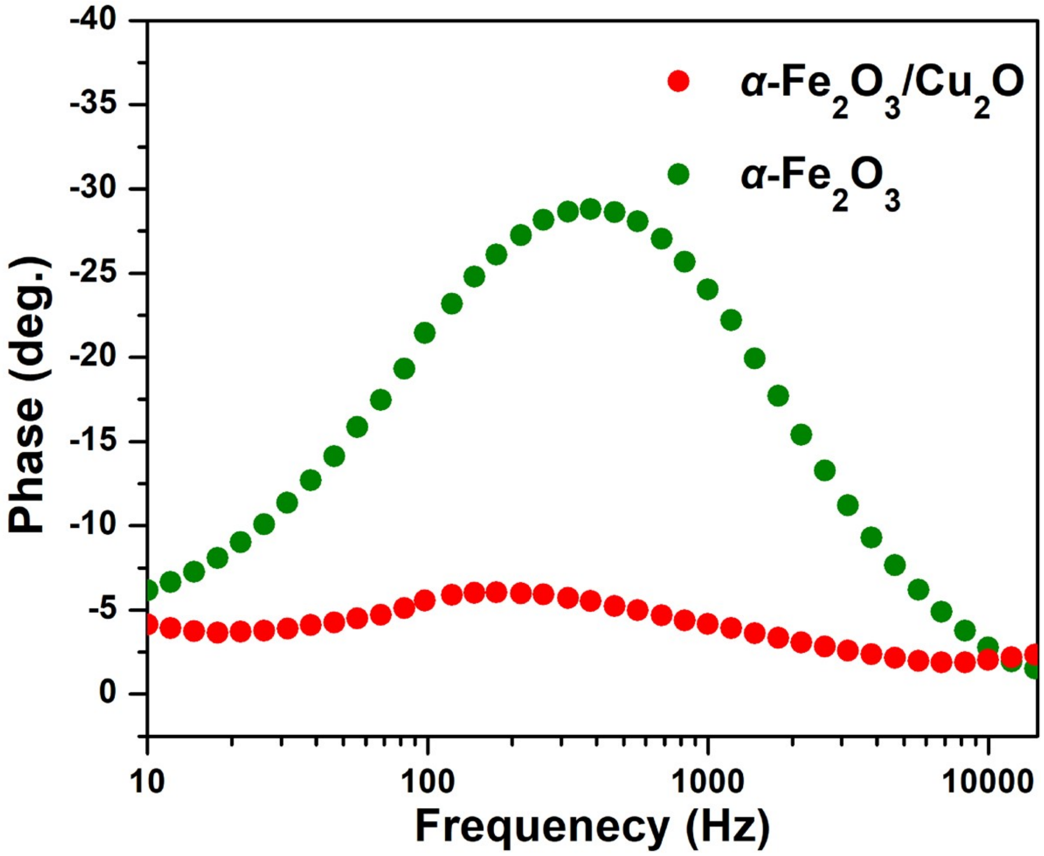

Fig. S8 Bode phase plots of α-Fe_2O_3 and α-Fe_2O_3/Cu_2O composite.

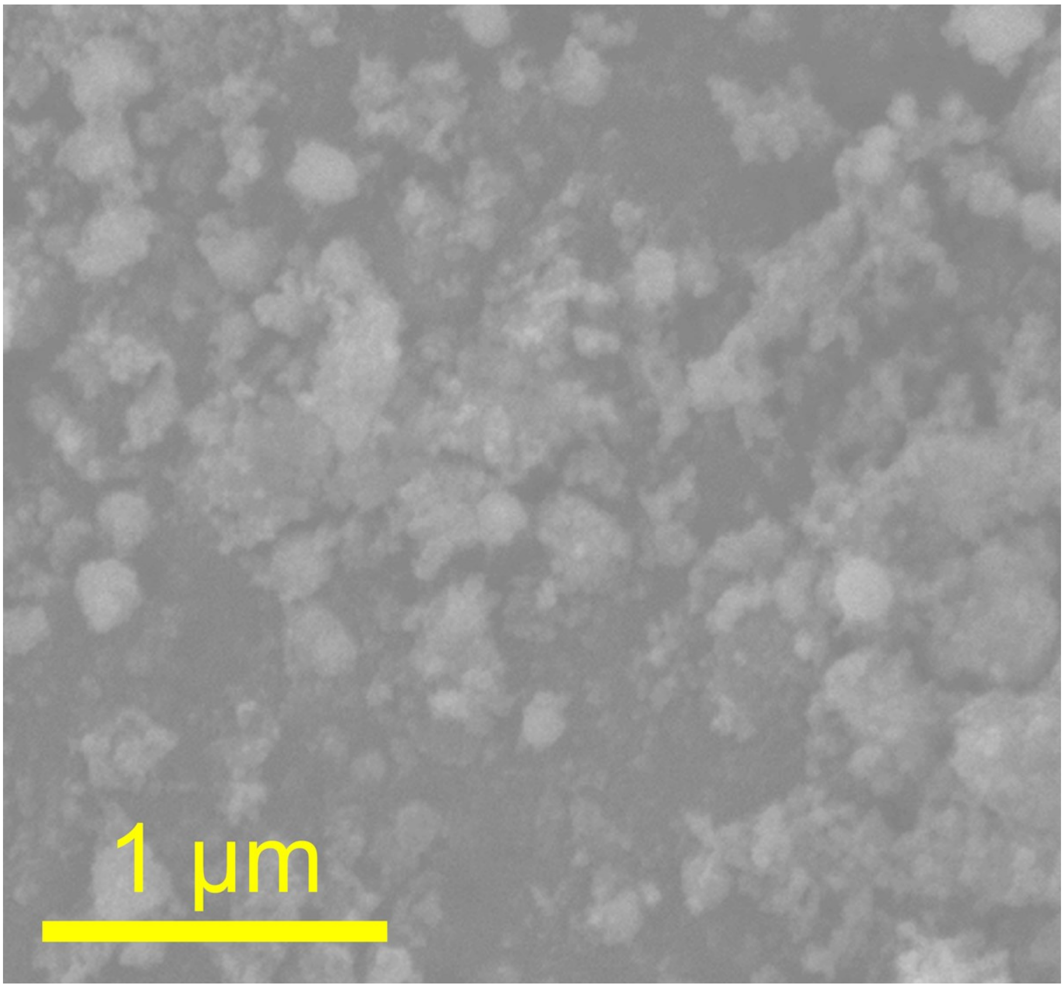

Fig. S9 SEM of α-Fe_2O_3/Cu_2O composite after the photocatalytic reactions.

Table S1. Oxidative coupling of primary amines with electron-withdrawing group in α-Fe_2O_3/Cu_2O

Entry	Substrate	Product	Yield [%]	Selectivity [%]
1	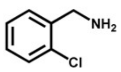	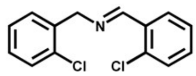	35.8	48.5
2	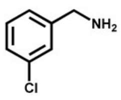	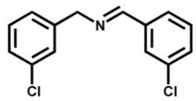	32.3	39.4
3	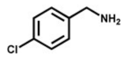	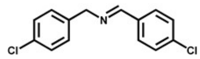	29.1	33.4
4	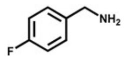	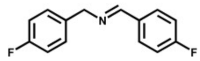	29.1	40.9

Table S2. The catalytic activity of photocatalyst in benzylamine oxidation coupled with hydrogen production

Entry	catalyst	Yield [%]	Selectivity [%]	H_2 rate [μmol g^{-1} h^{-1}]
1	α-Fe_2O_3/Cu_2O	69.3	89.7	1.2
2	no catalyst	5.8	10.3	0.1
3	dark	4.9	8.7	0.1
4	α-Fe_2O_3	9.8	16.8	0.3
5	Cu_2O	19.1	30.4	0.5

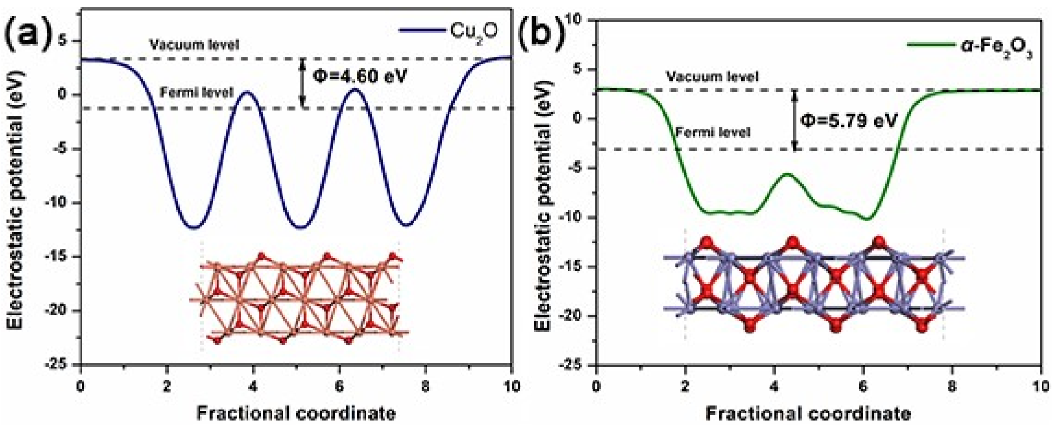

Fig. S10 DFT calculation results of α-Fe_2O_3 and Cu_2O

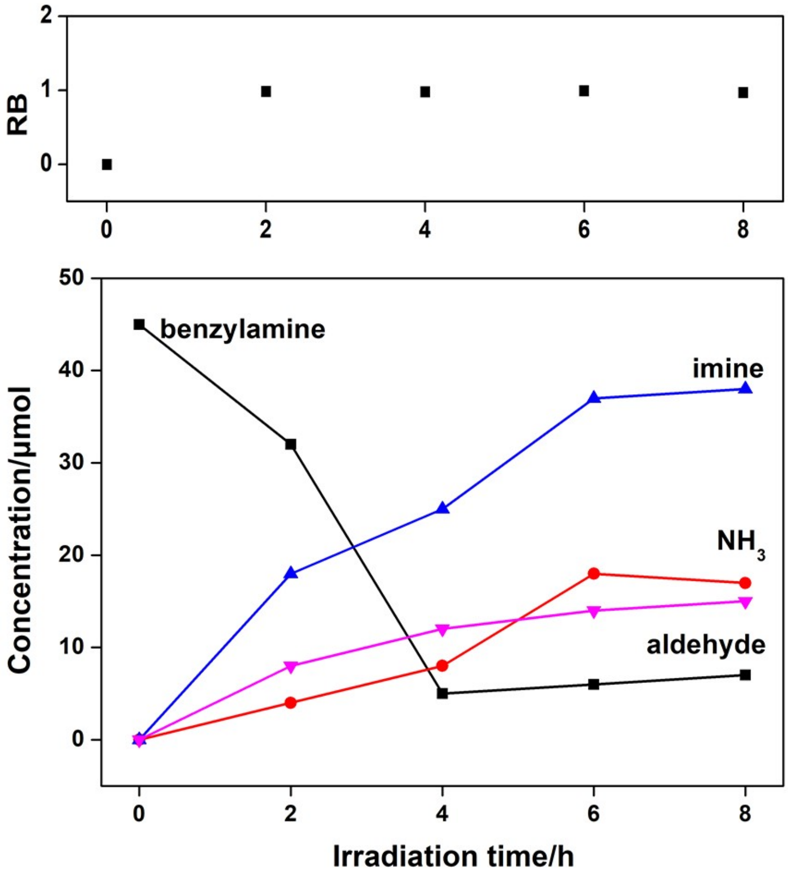

Fig. S11 Redox exploration diagram of primary amine oxidative coupling reaction[3]

Table S3. The AQE of α-Fe_2O_3/Cu_2O under different light irradiation

Wavelength (nm)	AQE (%)
450 nm	0.134
520 nm	0.124
600 nm	0.123

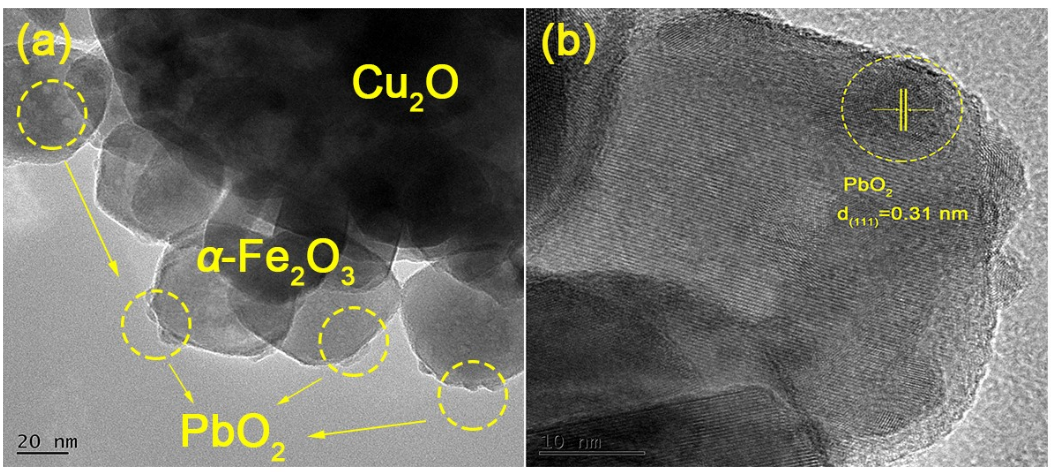

Fig. S12 The TEM of photodeposition of composite materials[4]

Table S4. Effect of different particle sizes on oxidative coupling reaction of primary amine

Entry	Size (nm)	Yield [%]	Selectivity [%]
1	300	69.3	89.7
2	400	53.8	72.3

Table S5. Effects of different light intensities on oxidative coupling of primary amines

Entry	Power [W]	Yield [%]	Selectivity [%]
1	5	3.4	10.2
2	20	46.7	67.2
3	50	69.3	89.7

References

[1] D. Zhu and Q. Zhou, *Appl. Catal. B-Environ.,* 2019, **19**, 118426-118436.

[2] J. Liu, W. Lu, Q. Zhong, X. Jin, L. Wei, H. Wu, X. Zhang, L. Li and Z. Wang, *Mol. Catal.,* 2017, **433**, 354-362.

[3] M. Fukui, A. Tanaka, H. Kominami, *ChemCatChem*, 2020, **12**, 3298-3305.

[4] Y. Peng, A. Rendón-Patiño, A. Franconetti, J. Albero, A. Primo, H. García, *ACS Appl. Energ. Mater.*, 2020, **3**, 6623-6632.